Available online at www.sciencedirect.com
ScienceDirect
Journal of Power Sources 163 (2006) 560–566
JOURNAL OF POWER SOURCES
www.elsevier.com/locate/jpowsour

Optimized electrochemical performance of $LiFePO_4$ at 60 °C with purity controlled by SQUID magnetometry

K. Zaghib [a,*], N. Ravet [b], M. Gauthier [c], F. Gendron [d], A. Mauger [e], J.B. Goodenough [f], C.M. Julien [d]

[a] *Institut de Recherche d'Hydro-Québec (IREQ), 1800 Bd Lionel-Boulet, Varennes, Que., Canada J3X 1S1*
[b] *Université de Montréal, CP 6128, Succursale centre-ville, Montréal, Que., Canada H3C 3J7*
[c] *Phostech Lithium, 135-D chemin du Tremblay, Boucherville, Que., Canada J4B7K4*
[d] *Institut des Nano-Sciences de Paris (INSP), UMR 7588, Université Pierre et Marie Curie, 140 rue de Lourmel, 75015 Paris, France*
[e] *Département MIPPU, CNRS, Campus Boucicaut, 140 rue de Lourmel, 75015 Paris, France*
[f] *The University of Texas at Austin, Austin, TX 78712, USA*

Received 31 July 2006; received in revised form 30 August 2006; accepted 15 September 2006
Available online 27 October 2006

Abstract

The local structure and magnetic properties of a series of carbon-coated $LiFePO_4$ particles prepared under different conditions are analyzed with X-ray diffractometry (XRD), FTIR and Superconducting Quantum Interference Device (SQUID) magnetometry for comparison. While nano-sized ferromagnetic particles (γ-Fe_2O_3 clusters) are detected by magnetic measurements in samples grown from iron(II) oxalate, such ferromagnetic clusters do not exist in the optimized samples grown from $FePO_4(H_2O)_2$. FTIR analyses show that carbon does not penetrate significantly inside the $LiFePO_4$ particles despite the fact that it has been very efficient in reduction of Fe^{3+} to prevent γ-Fe_2O_3 clustering, thus pointing to a gas-phase reduction process. The impact of the carbon coating on the electrochemical properties is also reported. No iron dissolution was observed after 200 charge–discharge cycles at 60 °C for cells containing lithium foil, lithium titanate or graphite negative electrodes.

Keywords: Lithium-ion batteries; Positive electrodes; Olivine structure; Magnetic properties; High-temperature performance

1. Introduction

Among the well-known Li-insertion compounds, the olivine $LiFePO_4$ compound is currently being investigated extensively as a positive electrode material for Li-ion batteries because of its low cost, low toxicity, and relatively high theoretical specific capacity of 170 mAh g^{-1} [1,2]. The current debate for the utilisation of $LiFePO_4$ in large-size batteries (for hybrid electric vehicles, for instance) is mainly focused on the perceived poor rate capability because of a low electronic conductivity. Another aspect concerns the material purity and the non-migration of iron ions through the electrolyte. The high-temperature performance is also a critical issue because batteries may be operated at elevated temperatures (around 60 °C). The early drawback of highly resistive $LiFePO_4$ has been resolved by coating the particle surface with carbon [3–5]. A seven-order-of-magnitude increase in the electronic conductivity is achieved by the addition of a carbon coat by using, for example, sucrose to produce carbon-coated $LiFePO_4$ (C-$LiFePO_4$) raw materials by a spray pyrolysis technique [6].

Recently, significant effort has been underway to improve $LiFePO_4$ by developing a new synthesis route via carbon coating [7]. The 1D Li channels make the olivine performance sensitive not only to particle size, but also to impurities and stacking faults that block the channels. Various types of iron-based impurities have been identified in the olivine framework: for example γ-Fe_2O_3, Fe_3O_4, $Fe_2P_2O_7$, Fe_2P, Fe_3P and $Fe_{75}P_{15}C_{10}$. The polyphosphate framework $Li_3Fe_2(PO_4)_3$ has also been identified [8]. Critical quality control of the product is necessary to obtain a complete understanding of synthesis conditions using combination of experiments such as Raman spectroscopy for an evaluation of the carbon film [9] and magnetic measurements, which are highly sensitive to a low impurity concentration [10,11].

In this paper, we report the results obtained on several samples of $LiFePO_4$ with special attention to the new generation

* Corresponding author. Tel.: +1 450 652 8019; fax: +1 450 652 8424.
E-mail address: zaghib.karim@ireq.ca (K. Zaghib).

0378-7753/$ – see front matter © 2006 Elsevier B.V. All rights reserved.
doi:10.1016/j.jpowsour.2006.09.030

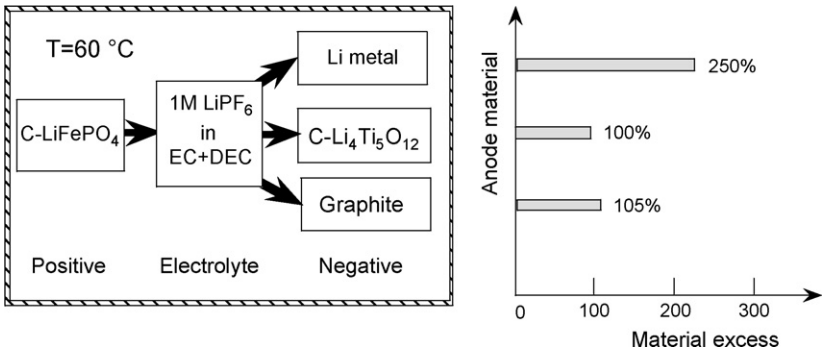

Fig. 1. Schematic representation of the procedure used to test the electrochemical performance of C-$LiFePO_4$ electrodes. All measurements were thermally carried out at temperature 60 °C. The graph (right panel) shows the excess of anode material used for each type of cell.

of phospho-olivine materials used in lithium cells operating at 60 °C. The magnetic properties are correlated with the electrochemical performance of the positive electrode materials. Magnetization and susceptibility measurements appear to be a powerful probes for impurity detection at very low concentration of trivalent iron (<1 ppm).

2. Experimental

Several $LiFePO_4$ samples were synthesized by solid-state reaction. The A-type $LiFePO_4$ specimens were prepared by mixing iron(II) oxalate [$Fe(C_2O_4)\cdot 2H_2O$], ammonium dihydrogen phosphate [$NH_4H_2PO_4$] and lithium carbonate [Li_2CO_3] in the molar ratio (1:1:1). The B-type samples were prepared from $FePO_4(H_2O)_2$ and Li_2CO_3. A stoichiometric amount of precursors was thoroughly mixed together in isopanol. After drying, the blend was heated at 700 °C for 8 h under reducing atmosphere. Carbon-coated C-$LiFePO_4$ was prepared with sucrose and cellulose acetate as the carbon precursors in acetone solution according to the following procedure. The carbon-free powder was mixed with the carbon precursors. The dry additive corresponded to 5 wt.% carbon in $LiFePO_4$. After drying, the blend was heated at 700 °C for 4 h under argon atmosphere. The quantity of carbon coat represents about 1 wt.% of the material (C-detector, LECO Co., CS 444). It should be noted that the choice of this moderate sintering temperature minimizes the amount of Fe^{3+} ions present in the powder since the presence of Fe^{3+} has been detected by Mössbauer experiments at sintering temperatures below 500 °C, and both trivalent Fe_2O_3 and $Li_3Fe_2(PO_4)_3$ are formed in such large quantities that they are detected by X-rays by sintering above 800 °C [12]. Nevertheless, we know from our prior work [9,10] that B-type $LiFePO_4$, even with an intermediate sintering temperature in the range 500–800 °C, does contain Fe_2O_3 nanoparticles, although in such small quantities that they can be detected only by investigation of magnetic properties.

The crystal structure of $LiFePO_4$ samples was analyzed by X-ray diffractometry (XRD) with a Philips X'Pert apparatus equipped with a Cu Kα X-ray source (λ = 1.5406 Å). XRD measurements were collected in the 2θ range 10–80°. Slice views were examined with a scanning electron microscope (SEM, Philips XL30). FTIR absorption spectra were recorded with a Fourier transform interferometer (model Bruker IFS113v) in the wavenumber range 150–1400 cm^{-1} at a spectral resolution of 2 cm^{-1}. The samples were ground to fine powders and dispersed into a CsI pellet in the proportion (1:300). Magnetic measurements (susceptibility and magnetization) were carried out with a fully automated magnetometer (MPMS-5S from Quantum Design) using an ultra-sensitive Superconducting Quantum Interference Device (SQUID) in the temperature range 4–300 K. The experimental details are given elsewhere [10]. The electrochemical properties of $LiFePO_4$ were measured at 60 °C in cells with metallic lithium as the negative electrode. The electrolyte was 1 M $LiPF_6$ in EC/DEC (1/1) solvent. The measurements were carried out following the experimental procedure previously described [13] using the coffee-bag technology developed at Hydro-Québec. Coffee-bag or laminated battery technology was described by Zaghib and Armand [14].

To study the capacity fade of $LiFePO_4$ at 60 °C, we used three different negative electrodes (Fig. 1), namely lithium metal, graphite and $Li_4Ti_5O_{12}$ (LTO). A lithium metal anode gave exact capacity during charge–discharge process with Li metal excess 2.5 times to $LiFePO_4$ cathode material. Due to the large excess of lithium metal, it was difficult to observe the capacity fade with this anode at 60 °C. Graphite anode was 5% of excess to $LiFePO_4$ cathode. This type of anode can detect easily the dissolution of iron because the passivation layer of graphite anode is ionic conductor and electronically insulator; so the dissolution of iron from the cathode side to the anode increases the electronic conductivity of passivation layer of graphite that results on the capacity fade of the cell. LTO has been used because it is passivation layer free and zero strain material. The anode has 0% excess to the cathode that gives the high stability of the cycling and also prevents side reactions or reduction of electrolyte to the potential of LTO (1.5 V versus Li^+/Li^0).

3. Results and discussion

3.1. Performance of optimized $LiFePO_4$

First, we present an overview of the high-temperature performance for an optimized B-type $LiFePO_4$ sample. The coffee-bag cell was charged and discharged at *C*/8 for the first cycle followed by 12 cycles at *C*/4 with 1 h rest before each charge and

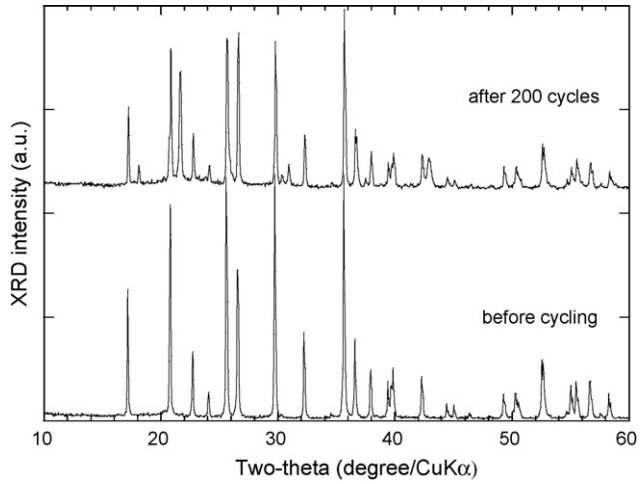

Fig. 2. XRD pattern of $LiFePO_4$ positive electrode before and after 200 cycles. Notice that the olivine framework (*Pmna* space group) remains intact after cycling at 60 °C.

discharge. This high-temperature test was made at 60 °C, which is the appropriate condition to investigate possible iron dissolution in non-aqueous electrolytes. Fig. 2 shows the XRD patterns of the new generation of $LiFePO_4$ after 200 cycles (47 days) at 60 °C. There is no change in the olivine structure after cycling at 60 °C. We observed Bragg lines with the same intensity as that for the pristine material. The capacity loss was below 3% in 100 cycles for this optimized electrode material, which also displays excellent capacity retention.

A close examination was made for the detection of any iron dissolution that could occur after long-term cycling. The analysis of iron species was investigated at the separator/lithium (SL) interface by SEM cross-section (slice view) as shown in Fig. 3a–c. The micrograph (Fig. 3a) obtained from evaluation of the earlier generation material shows the presence of iron islands at the SL interface. Obviously, some iron particles (or ions) migrate through the electrolyte from the $LiFePO_4$ positive electrode to the lithium negative. The net effect of this migration is a large decrease in capacity retention of the Li//$LiFePO_4$ cell. Fig. 3b shows a micrograph obtained from tests with an optimized electrode in a Li cell with a lithium foil negative. In this case, there is no iron detected at the SL interface, which remained intact after 100 cycles. In fact, this high performance was possible not only because the optimized synthesis of the $LiFePO_4$ powders, but also because of strict control of the structural quality of the materials. Several physical methods were utilized to analyze the local structure and the electronic properties of the phospho-olivine framework. Fig. 3c shows the SEM picture of graphite taken from a Li-ion cell after 200 cycles. No iron was observed at the surface of the electrode material. EDX analysis of the graphite electrode shown in Fig. 4 confirms this last observation. Iron dissolution if it occurred should be evident in the EDX spectrum on the graphite side. In addition, elemental analysis of the electrolyte in the Li-ion cell was carried out by the ICP technique to detect of iron after 200 cycles. No iron, even at the ppm level, was found in the electrolyte solution. Thus, all these data converge to the conclusion that $LiFePO_4$ is not soluble at 60 °C with the optimized material.

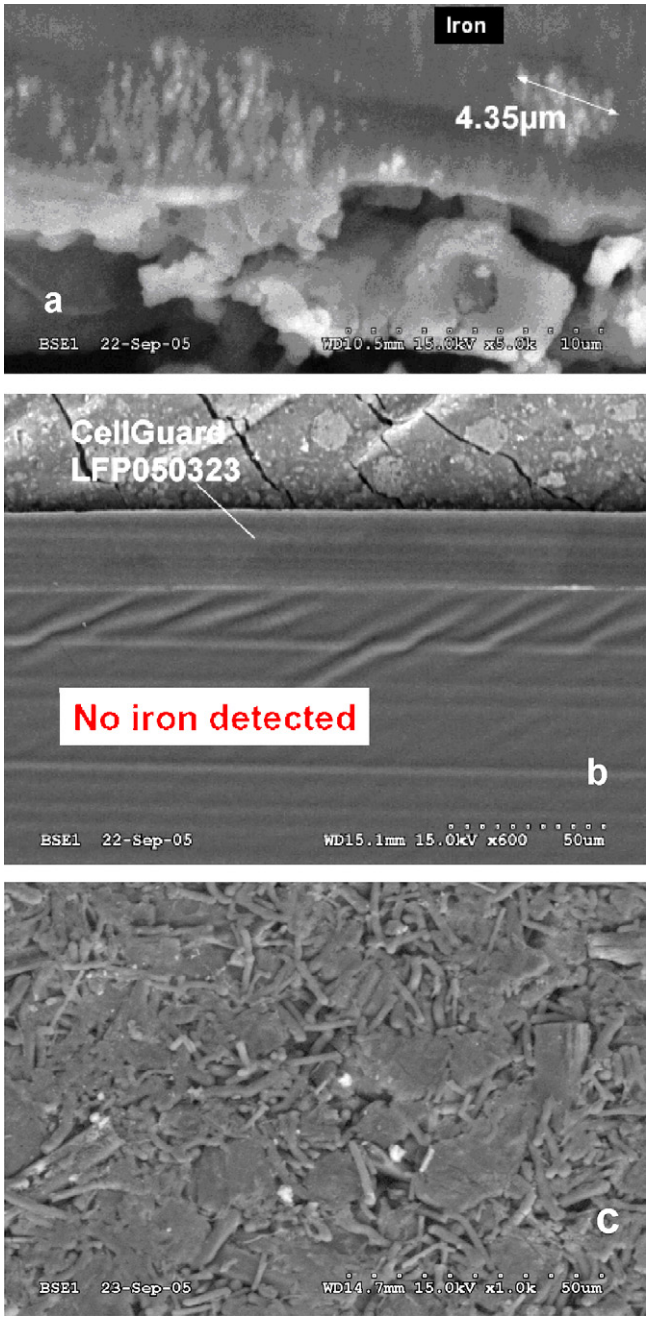

Fig. 3. Post-mortem SEM images of the detection of iron species at the separator/lithium interface. (a) Image showing the formation of iron islands at the interface with an earlier generation of $LiFePO_4$. (b) No iron was detected at the surface of lithium foil with the optimized $LiFePO_4$. (c) Li-ion graphite electrode after 200 cycles does not show the presence of iron particle.

The electrochemical properties of $LiFePO_4$ are known to be sensitive to the mode of preparation and the structural properties. This can be an advantage for potential applications since it allows for an optimization of the material if we can correlate the mode of preparation with the structural and the physical properties.

To address this issue, we investigated this relationship in $LiFePO_4$ sample that were grown at different conditions. Undesirable impurities in the lattice can be introduced during the growth process. For instance, the presence of Fe_2P can increase

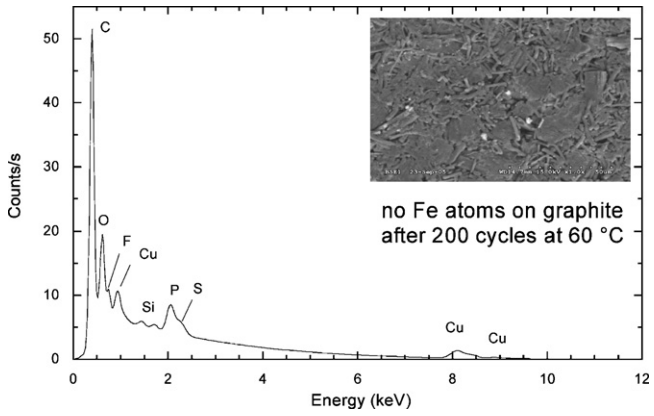

Fig. 4. EDX analysis of a Li-ion graphite electrode after 200 cycles at 60 °C. Elemental analysis does not indicate the presence of iron.

the electronic conductivity, but on the other hand it also decreases the ionic conductivity so that both the capacity and cycling rates are degraded with respect to CC-$LiFePO_4$. Furthermore, we know that hydrogen, carbon monoxide, or carbon can reduce Fe_2O_3 through different reduction steps that depend on temperature and other physical parameter such as particle size. Although we anticipate that over 1000 °C carbon might reduce Fe^{3+} ions or through the formation of CO gas to prevent the formation of γ-Fe_2O_3, other factors may be involved. We believe that the carbon deposition process, which was organic precursors to make C-coated samples, generates a reductive gas such as hydrogen that is more kinetically active and reduces Fe^{3+} impurities in the 400–700 °C temperature range used in our studies. This model is also favoured by the fact that the organic precursor is usually mixed with the $LiFePO_4$ material or with the $LiFePO_4$ chemical precursors by solution processes at a molecular-size level. In Section 3.2, we investigate the physical properties of several $LiFePO_4$ powders for which a small amount of impurities has been detected. Their fingerprints are reported as follows.

3.2. The local structure of $LiFePO_4$

Infrared spectroscopy probes bulk properties [15,16]; the amount of carbon in $LiFePO_4$ is too small to be detected by such experiments [17]. The vibrational modes of $LiFePO_4$ are primarily due to motion associated with phosphate and iron, the other modes show some lithium contribution. The FTIR spectra of several $LiFePO_4$ samples in the low-wave number region (300–600 cm^{-1}) involving bending modes and in the high-wave number domain (600–1300 cm^{-1}) involving stretching vibrations are shown in Fig. 5a and b, respectively. A comparison can be established between impurity-containing samples (A-type samples) and the optimized phospho-olivine material (sample B-10). In the low-wave number region of the active symmetric and asymmetric (ν_2–ν_4) bending modes of P–O bonds, we observe two well-resolved doublets at 349–377 and 468–500 cm^{-1} for the optimized CC-$LiFePO_4$ (Fig. 5a). When an impurity such as lithium phosphate (sample A-01) is present, the FTIR spectrum displays some modifications in the shape of the doublets and

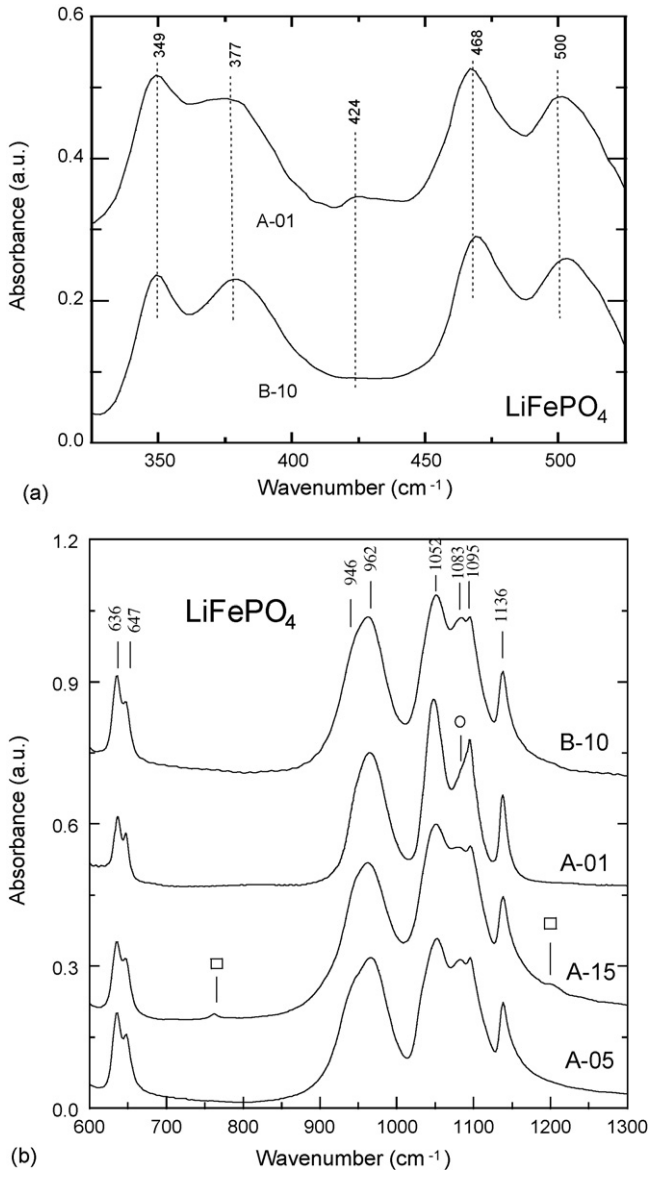

Fig. 5. FTIR spectra of $LiFePO_4$ samples. (a) Low-wave number region showing the band at 424 cm^{-1} due to Li_3PO_4 impurity in the A-01 sample. (b) High-wave number region displays bands due to Li_3PO_4 (◯) and $LiFeP_2O_7$ (□). The best $LiFePO_4$ material is the B-10 sample (upper curve).

an additional IR band grows at 424 cm^{-1} that is the vibrational signature of Li_3PO_4.

The presence of an impurity was also observed in the high-wave number region (Fig. 5b) of the symmetric and asymmetric (ν_1–ν_3) modes of PO_4 groups. Introduction of $LiFeP_2O_7$ is detected by the appearance of two sets of IR bands at 762 and 1180 cm^{-1}. The band at 762 cm^{-1} is due to the symmetric stretching mode of P_2O_7 pyrophosphate groups, while the high-frequency band at 1180 cm^{-1} is assigned to the vibration of the PO_3 terminals [17–19]. These two spectral features are fingerprints of the diphosphate impurity. The inclusion of Li_3PO_4 is observed by additional spectral features such as enhancement of the asymmetric stretching (ν_3) vibration of $(PO_4)^{3-}$ oxo-anions. It is worth noting that FTIR measurements (like X-ray diffractometry) are not sensitive to detect of low concentrations

of impurities (at the ppm level). The FTIR features show that the carbon does not penetrate significantly inside the $LiFePO_4$ particles, although it is very efficient in reducing Fe^{3+}, which prevents γ-Fe_2O_3 clustering, thus pointing to a gas-phase reduction process. For these reasons, we describe in Section 3.3 the magnetic experiments that are very useful to detect low concentration [10].

3.3. Magnetic properties of $LiFePO_4$

The magnetic properties of $LiFePO_4$ were reported in an earlier publication by Santoro and Newnham [20]. The material undergoes a transition to antiferromagnetic order at a Néel temperature $T_N = 50\,^{\circ}C$. Fig. 6 shows the isothermal plots of the magnetic moment versus applied magnetic field for A-type and optimally synthesized $LiFePO_4$ (B-type). From these results, we clearly observe a difference between the magnetic properties of the phospho-olivine materials. The B-$LiFePO_4$ sample displays a linear variation in its $M(H)$ curve, while a non-linear behaviour is observed at low-magnetic field for the A-type $LiFePO_4$. This curvature is signature of ferromagnetic impurities [10,11]. While nano-sized ferromagnetic particles were evidenced in previously prepared $LiFePO_4$, such clusters do not exist in the optimized $LiFePO_4$. These results illustrate that the magnetization $M(H)$ is the superposition of two contributions $M(H) = \chi_m H + M_{extrin}$. The intrinsic part, $\chi_m H$, that is linear in the applied magnetic H and an extrinsic component, $M_{extrin} = Nn\mu\pounds(\xi)$, that is easily saturated by the application of H and is due to ferromagnetic impurities. Here, $\pounds(\xi)$ is the Langevin function, N is the number of magnetic clusters, and each cluster is made of n magnetic moments μ.

Analysis of the A-type samples of Fig. 6, however, gives an average separation of the magnetic clusters that is too large for interaction between particles (superparamagnetic model). This hypothesis must be released where the number n of magnetic clusters is so large that magnetic interactions between the ferrimagnetic particles become important [9]. At high fields, M_{extrin} saturates to $Nn\mu$ so that this quantity is readily determined as the ordinate at $H = 0$ of the intersection of the tangent to the magnetization curves at large fields. As a result, we find that $Nn\mu$ does not depend significantly on temperature below 300 K. We are in the situation where the cluster magnetization is temperature independent, which amounts to say that the Curie temperature T_c inside the clusters is much larger than 300 K. This is important information on the nature of the ferromagnetic clusters. In particular, this feature precludes the existence of Fe_2P clusters in some $LiFePO_4$ samples prepared according to a different procedure [10], since the Curie temperature of these clusters is only 220 K. The nature of the strongly ferromagnetic clusters in the present case is most likely maghemite (γ-Fe_2O_3).

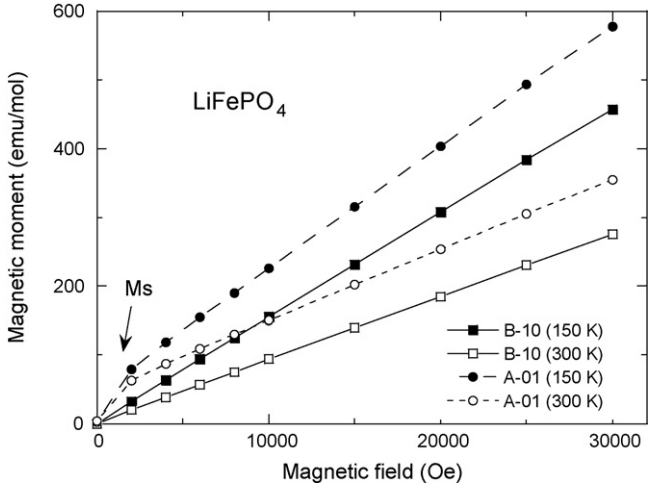

Fig. 6. Isothermal curves of the magnetic moment vs. applied magnetic field for A-type and optimized (B-type) $LiFePO_4$.

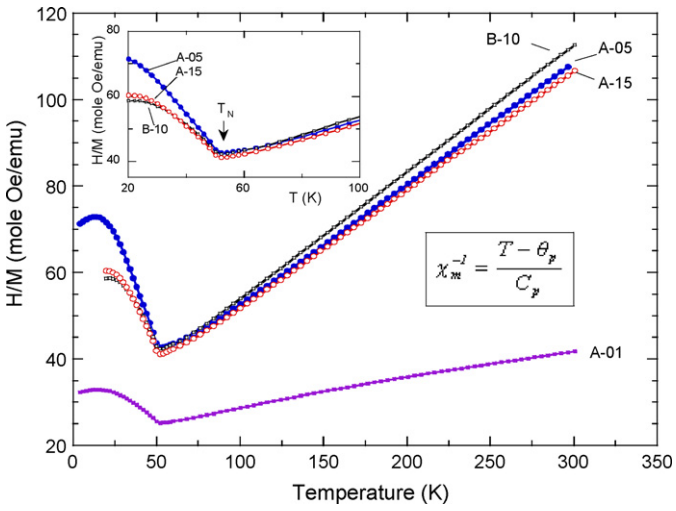

Fig. 7. Temperature dependence of the reciprocal magnetic susceptibility of $LiFePO_4$ samples. The best material (B-10) displays the lowest Curie constant 3.41 emu K mol^{-1}. Insert shows the cusp of the transition from antiferromagnetic ordering to the paramagnetic range at $T_N = 52$ K.

The combination of ESR spectroscopy (not presented here) and SQUID magnetometry shows that the fraction of iron in the Fe^{3+} configuration falls to a residual impurity concentration lower than a few tenths of a ppm. This is the net result of the thermal effect, the carbon coating and also the careful selection of the Fe^{3+} precursor [8]. The other structural properties show that carbon does not penetrate significantly inside the $LiFePO_4$ nano-sized particles. The carbon deposit can also be characterized by Raman scattering [21].

Fig. 7 shows the temperature dependence of the reciprocal magnetic susceptibility of $LiFePO_4$ samples. The curves $\chi_m^{-1}(T)$ are in quantitative agreement with a prior work [20]. The insert shows the cusp of the transition from antiferromagnetic ordering to the paramagnetic range at $T_N = 52$ K. It is remarkable that the A-type sample displays different magnetic features due to the existence of ferrimagnetic impurities. The first consequence is an ambiguity in what is called the magnetic susceptibility χ_m since M/H is distinct from dM/dH. The magnetic susceptibility measured with a SQUID at $H = 10$ kOe shows the non-linearity of the magnetic moments, which is due to the presence of γ-Fe_2O_3. The best material (B–20 sample) shows the lowest Curie constant 3.41 emu K mol^{-1}. The effective magnetic moment $\mu_{eff} = 5.22\,\mu_B$ is close to theoretical value $4.90\,\mu_B$ calculated from the spin-only value of Fe^{2+} in its high-spin configuration. Departure from the spin-only value may reflect the presence of

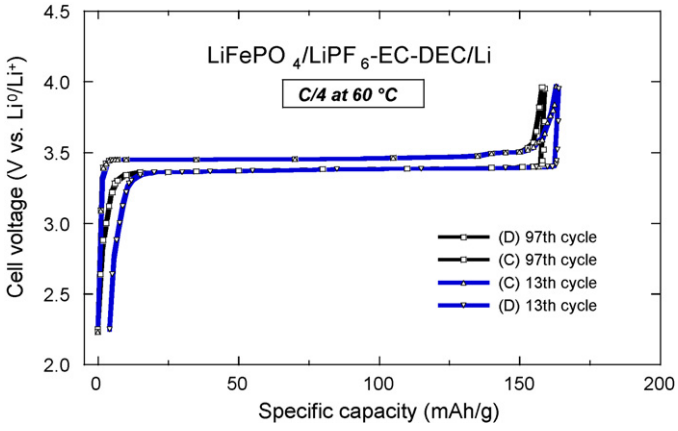

Fig. 8. Electrochemical performance of the C-$LiFePO_4$/$LiPF_6$-EC-DEC/Li cells at 60 °C. Charge–discharge cycling was conducted at the *C*/4 rate.

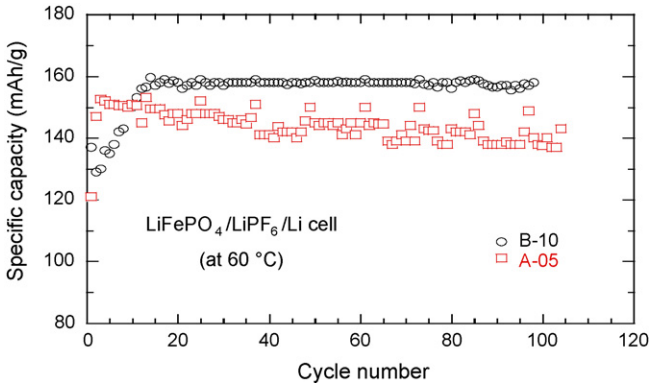

Fig. 9. Specific capacity vs. cycle life for C-$LiFePO_4$/$LiPF_6$-EC-DEC/Li cells at 60 °C. The optimized $LiFePO_4$ electrode (B-10) is compared with the earlier generation electrode (A-05).

Fe^{3+} ions and/or an orbital-momentum contribution from the Fe^{2+} ions [22].

3.4. Electrochemical performance at 60 °C

Fig. 8 presents the typical electrochemical performance of C-$LiFePO_4$/$LiPF_6$-EC-DEC/Li cells at 60 °C. The charge–discharge curves were obtained by cycling at *C*/4 rate (about 35 mA g^{-1}) in the voltage range 2.2–4.0 V versus Li^0/Li^+. The optimized $LiFePO_4$ exhibits a reversible capacity that is maintained over many charge–discharge cycles. The 13th and 97th cycle shows a similar specific capacity of 160 mAh g^{-1}. These results illustrate the excellent electrochemical performance of the carbon-coated olivine material. The electrode can be fully charged up to 4 V, which is its most reactive state. This remarkable performance is attributed to the optimized carbon-coated particles and their structural integrity under a large current in the electrode. Even at such a high cycling rate, C-$LiFePO_4$ exhibits rapid kinetics of lithium extraction, and realizes most of its theoretical capacity (170 mAh g^{-1}). The discharge profile appears with the typical voltage plateau (at ca. 3.45 V versus Li^0/Li^+) attributed to the two-phase reaction of the $(1-x)FePO_4 + xLiFePO_4$ system.

A comparison of the specific capacity between A-type $LiFePO_4$ and B-type $LiFePO_4$ electrodes during long-term cycling is shown in Fig. 9. The cycling performance for the new generation of CC-$LiFePO_4$ material is excellent at 60 °C. After 100 cycles at *C*/4 rate, and with a typical cut-off voltage 4.0–2.2 V, a constant capacity was observed. This best performance is due to the improved technology used in electrode fabrication, i.e. improvements in the nature and the morphology of the carbon-coating and the optimization of the particle size of the olivine phase. These are the two main factors controlling the electrode performance. In our previous exploration of the surface properties of the $LiFePO_4$ particle, we have shown by Raman spectroscopy that the deposit is a disordered graphite-type carbon [22]. The small amount of carbon (<2 wt.%) can be viewed as a film of irregular thickness, 30 nm thick on average, with gaps. The above experimental condition (ca. 60 °C) has a severe impact on the kinetics of the Fe^{2+}/Fe^{3+} redox reaction, but the recent report from Hydro-Québec Research Labs (IREQ) showed that this type of C-$LiFePO_4$ electrode can be cycled at 60 °C without significant capacity loss for over 200 cycles [7]. Optimized particle size in the range 200–300 nm agrees well with the average diameter of grains *L* that validates the characteristic diffusion time $\tau = L^2/4\pi^2 D^*$ [23], where D^* is the chemical diffusion coefficient of Li^+ ions in the $LiFePO_4$ matrix (typically 10^{-12} cm^2 s^{-1}) when compared with the experimental discharge rate up to 5 C.

The electrochemical performance of C-$LiFePO_4$ was tested in various cell configurations with lithium foil, graphite and carbon-coated lithium titanate C-$Li_4Ti_5O_{12}$ (LTO) as negative electrodes. Figs. 10 and 11 show the cycling behaviour of cells with three different materials as negative electrodes. The cells were cycled at 60 °C in the potential range 2.5–4.0 V. The discharge capacity and electrochemical utilisation, i.e. the ratio discharge/charge, versus cycle number are excellent for the C-$LiFePO_4$/$LiPF_6$-EC-DEC/Li cells discharged at 1 C and charged at *C*/6 (Fig. 10). Similar results are shown for cells with graphite (Fig. 11a) and C-$Li_4Ti_5O_{12}$ negative electrodes (Fig. 11b). These Li-ion cells provide coulombic efficiencies 99.9 and 100%,

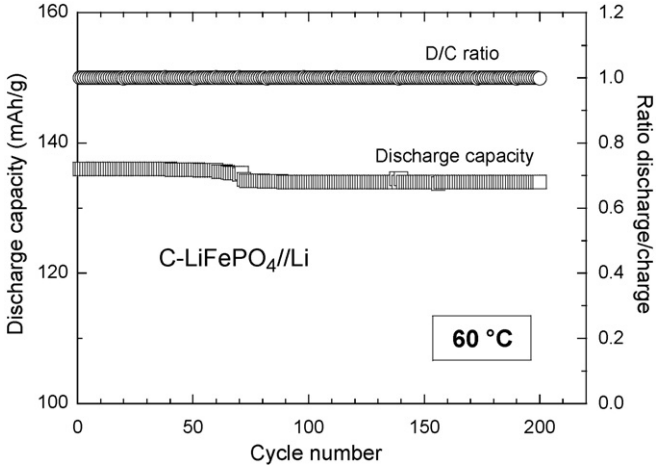

Fig. 10. Discharge capacity and discharge/charge ratio (electrochemical utilisation) vs. cycle number for C-$LiFePO_4$/$LiPF_6$-EC-DEC/Li cells at 60 °C. Cells were discharged at 1 C and charged at *C*/6 in the potential range 2.5–4.0 V.

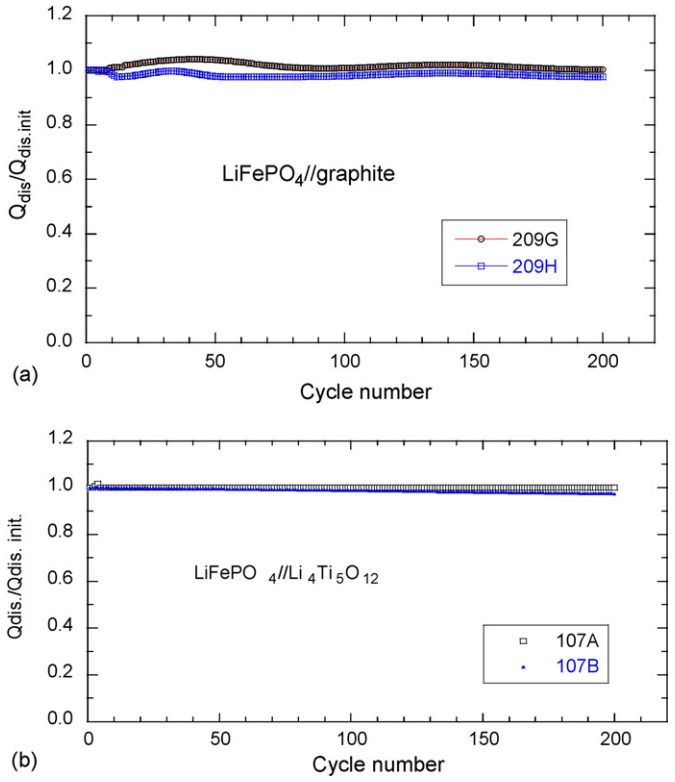

Fig. 11. Plots of the ratio between the current discharge capacity and the initial capacity vs. cycle number for Li-ion cells cycled at 60 °C with graphite (a) and C-$Li_4Ti_5O_{12}$ (b) electrodes. Cells were discharged at 1 C in the potential range 2.5–4.0 V.

respectively. Plots of the ratio between the current discharge capacity and the initial capacity versus cycle number indicate a constant capacity retention at 60 °C. No capacity fade was observed after 200 cycles with lithium, LTO and graphite.

A recent study at Lawrence Berkeley National Laboratory showed the impact of different strategies to alleviate the problem of poor conductivity and slow diffusion in the $LiFePO_4$ solid phase [24]. We made a similar investigation to evaluate the performance of C-$LiFePO_4$ at different rates of charge and discharge. Measurements carried out in the range from *C*/4 to 10 C (based on a capacity of 170 mAh^{-1}) shows that at the high rate of 4 C, the Li//CC-$LiFePO_4$ cell delivers a discharge capacity of 130 mAh g^{-1}. Clearly, some treatment of the C-$LiFePO_4$, i.e. deliberate in situ carbon coating, is necessary for adequate performance of $LiFePO_4$.

4. Conclusion

In this work, we compared the physical and electrochemical properties of a series of carbon-coated $LiFePO_4$ samples. As shown by FTIR spectroscopy, carbon does not penetrate into $LiFePO_4$. Nevertheless, a major effect of the carbon deposition process has been to reduce Fe^{3+}, most probably through a gas-phase reduction process involving hydrogen from the organic carbon precursor. The hydrogen prevents formation of γ-Fe_2O_3 nanoparticles in which iron is in the trivalent state. The magnetic measurements indicated that nanoparticles of γ-Fe_2O_3 at a concentration of 0.7 ppm are present in the A-type sample, such clusters are simply not observed in the new generation of carbon-coated sample (B-type). Thus, this study demonstrates that magnetic measurements (combination of $M(H)$ and $\chi(T)$ data) are beneficial for detecting ferric and/or ferrous impurities, as well as for the quality control of $LiFePO_4$. Electrochemical tests have been conducted under various conditions to assess the influence of the electrolyte on stability and the influence of electrode processing. Post-mortem analysis, i.e. ICP, XRD, SEM, showed that no iron species were detected at the separator-negative electrode interface in cells with lithium metal, graphite and C-$Li_4Ti_5O_{12}$. This result is attributed to the high quality of the "optimised" $LiFePO_4$, impurity-free materials used as positive electrodes.

References

[1] A.K. Padhi, K.S. Nanjundaswamy, J.B. Goodenough, J. Electrochem. Soc. 144 (1997) 1188.
[2] N. Ravet, Y. Chouinard, J.F. Magnan, S. Besner, M. Gauthier, M. Armand, J. Power Sources 97–98 (2001) 503.
[3] N. Ravet, A. Abouimrane, M. Armand, Nat. Mater. 2 (2003) 702.
[4] N. Ravet, S. Besner, M. Simoneau, A. Vallée, M. Armand, J.F. Magnan, US Patent 6,962,666 (2005).
[5] Y. Hu, M.M. Doeff, R. Kostecki, R. Finones, J. Electrochem. Soc. 151 (2004) A1279.
[6] S.L. Bewlay, K. Konstantinov, G.X. Wang, S.X. Dou, H.K. Liu, Mater. Lett. 58 (2004) 1788.
[7] K. Zaghib, V. Battaglia, P. Charest, V. Srinivasan, A. Guerfi, R. Kostecki, IBA-HBC Meeting, Wailoloa, Hawaii, 2006, Extend abstract 35.
[8] A. Ait Salah, P. Jozwiak, J. Garbarczyk, F. Gendron, A. Mauger, C.M. Julien, Ext. Abstracts of the 207th ESC Meeting, Québec-City, 2005, Extend abstract 1343.
[9] M.M. Doeff, Y. Hu, F. McLarnon, R. Kostecki, Electrochem, Solid State Lett. 6 (2003) A207.
[10] A. Ait Salah, A. Mauger, F. Gendron, C.M. Julien, Phys. Status Solidi (a) 203 (2006) R1.
[11] A. Ait-Salah, A. Mauger, C.M. Julien, F. Gendron, Mater. Sci. Eng. B 129 (2006) 232.
[12] A. Yamada, S.C. Chung, K. Hinokuma, J. Electrochem. Soc. 148 (2001) A224.
[13] K. Zaghib, J. Shim, A. Guerfi, P. Charest, K.A. Striebel, Electrochem. Solid State Lett. 8 (2005) A207.
[14] K. Zaghib, M. Armand, Canadian Patent CA2,411,695 (2002).
[15] M.T. Paques-Ledent, P. Tarte, Spectrochim. Acta, Part A 30 (1974) 673.
[16] C.M. Burma, R. Frech, J. Electrochem. Soc. 151 (2004) A1032.
[17] A. Ait-Salah, P. Jozwiak, J. Garbarczyk, K. Benkhouja, K. Zaghib, F. Gendron, C.M. Julien, J. Power Sources 140 (2005) 370.
[18] R. Bacewicz, P. Woroniecki, J. Garbarczyk, Phys. Chem. Glasses 40 (1999) 124.
[19] A. Adamczyk, M. Handke, W. Mozgawa, J. Mol. Struct. 511–512 (1999) 141.
[20] R.P. Santoro, R.E. Newnham, Acta Crystallogr. 22 (1967) 344.
[21] R. Kostecki, B. Schnyder, D. Alliata, X. Song, K. Kinoshita, R. Kotz, Thin Solid Films 396 (2001) 36.
[22] A. Ait Salah, A. Mauger, K. Zaghib, J.B. Goodenough, N. Ravet, M. Gauthier, F. Gendron, C.M. Julien, J. Electrochem. Soc. 153 (2006) A1692.
[23] W. Weppner, R.A. Huggins, J. Electrochem. Soc. 124 (1977) 1569.
[24] K. Striebel, J. Shim, V. Srinivasan, J. Newman, J. Electrochem. Soc. 152 (2005) A664.